

Article

Effect of Different Nano-Sized Silica Sols as Supports on the Structure and Properties of Cu/SiO₂ for Hydrogenation of Dimethyl Oxalate

Chuancai Zhang ¹, Denghao Wang ², Mingyuan Zhu ², Feng Yu ² and Bin Dai ^{2,*}

¹ School of Chemical Engineering and Technology, Tianjin University, Tianjin 300072, China; zhangchuanc111@126.com

² School of Chemistry and Chemical Engineering of Shihezi University, Shihezi 832000, China; JayGatsby@stu.shzu.edu.cn (D.W.); zhumin yuan@shzu.edu.cn (M.Z.); yufeng05@mail.ipc.ac.cn (F.Y.)

* Correspondence: db_tea@shzu.edu.cn; Tel.: +86-993-205-7277

Academic Editors: Adam F. Lee, Jean-Philippe Dacquin and Karen Wilson

Received: 6 January 2017; Accepted: 20 February 2017; Published: 25 February 2017

Abstract: Cu/*x*-SiO₂ catalysts with 4, 10, and 20 nm silica sols as supports was produced by ammonia evaporation method and characterized. Different nano-sized silica sols as supports significantly affected the structure and catalytic properties of the copper catalysts for ethylene glycol synthesis from dimethyl oxalate. Compared with Cu/20-SiO₂ and Cu/4-SiO₂ catalysts, the catalytic performance and stability of Cu/10-SiO₂ catalyst were greatly enhanced. The Cu/10-SiO₂ catalyst showed 99.9% conversion with 94% EG selectivity and a lifetime of over 3080 h if it is calculated by industrial weight liquid hourly space velocity (WLHSV) of 0.5 h⁻¹. The Cu/10-SiO₂ catalyst has one of the longest lifetimes among the catalysts and is a good alternative catalyst for this reaction. Improvement in the catalytic performance and stability of Cu/10-SiO₂ is attributed to the proper *S*_{BET}, *D*_p and larger dispersion of copper. In addition, the supports of Cu/10-SiO₂ catalyst have smaller particles than that of Cu/20-SiO₂; thus, the migration and growth of copper species in catalysts are restrained during the reaction.

Keywords: silica sol; ethylene glycol; hydrogenation; stability; lifetime

1. Introduction

Chemical catalytic hydrogenation of ester is an important method for the production of high value-added intermediates and fine organic products [1–3]. One of the representative reactions is the synthesis of ethylene glycol (EG) by using coal as raw material via dimethyl oxalate (DMO) hydrogenation. The coal-DMO-EG process has gained interest and rapid development because of the increasing use of EG [4], especially in China where oil resource is scarce and coal resource is abundant. Several disadvantages of this process, such as low yields and short lifetime of catalyst for hydrogenation of DMO to EG, should be solved. Catalysts based upon copper have been extensively studied and believed to be effective for the hydrogenation of DMO to EG [5]. However, problems in copper catalyst such as sintering, poisoning, and carbon deposition still exist. The aggregation and growth of active copper particles is one of the most important causes for catalyst deactivation. Improving the activity and stability of the DMO hydrogenation catalyst to enhance EG synthesis is crucial.

The support greatly influences the dispersion of active component in catalysts and the bonding strength with the active element. Increasing the dispersion of active copper and bond strength between support and active component is beneficial for preventing the agglomeration and sintering of active copper. Silica [6,7], alumina [8], zirconia [9], titania [10], and other supports [11,12] can be used for

this reaction, and the supports containing silica are considered to be the most suitable supports. Silica sol, HMS [13], MCM-41 [14], HZSM [15], and SBA-15 [16] have been widely studied. Investigation on HMS, SBA-15, HZSM, and so on are mainly concentrated on the influence of the mesoporous structure on the catalyst. As for silica sol, research only refers to 20 nm silica sol without considering the influence of smaller-sized silica sol. Relevant reports on the effect of different nano-sized silica sol as the support on the structure and properties of copper-based catalysts are still lacking.

In the present work, ammonia evaporation was utilized for the production of 4, 10, and 20 nm silica sols as the supports in Cu/*x*-SiO₂ catalysts for EG synthesis from DMO. The catalytic stability and activity of Cu/10-SiO₂ catalyst were enhanced significantly compared with Cu/20-SiO₂ and Cu/4-SiO₂ catalysts. The effect of different nano-sized silica sols as the supports on the texture and properties of Cu/*x*-SiO₂ catalysts was systemically investigated according to various analytical techniques. Texture changes and improvements in catalytic stability caused by the effect of nano-sized supports in the catalyst were discussed with the characterization and experimental results.

2. Results and Discussion

2.1. Physicochemical Properties

The physicochemical properties of Cu/*x*-SiO₂ are listed in Table 1. A series of Cu/*x*-SiO₂ catalysts with Cu loading (theoretical content is 20 wt %) but different nano-sized silica sol as supports was prepared by Auger electron (AE) method. The actual Cu loading in the calcined catalysts measured by ICP-AES ranged from 16.1% to 17.5%, which was lower than the pre-set value (20%), indicating that most of the copper was deposited onto the catalyst except for a small residual copper in the solution. The actual load of copper in the catalyst tended to decrease with the increasing nanoparticle size of the silica sol. The smaller the particle size of silica sol, the more copper is adsorbed in the catalysts.

Table 1. Physicochemical properties of the catalysts.

Sample	Cu loading (wt %) ^a	Cu Dispersion (%) ^b	S _{Cu} ^b (m ² ·g ⁻¹)	S _{BET} (m ² ·g ⁻¹)	V _p (cm ³ ·g ⁻¹)	D _p (nm)	d _{Cu20(111)} (nm) ^c	d _{Cu} (nm) ^d
Cu/4-SiO ₂	17.5	25.7	30.5	472.7	1.05	4.6	3.3	4.4
Cu/10-SiO ₂	16.8	23.9	27.2	349.4	0.77	8.8	3.8	5.4
Cu/20-SiO ₂	16.1	20.1	21.9	244.9	0.59	9.7	4.5	5.8
Cu/4-SiO ₂ -used	17.3	-	-	274.3	0.69	6.5	-	5.9
Cu/10-SiO ₂ -used	16.7	-	-	257.9	0.61	9.7	-	6.1
Cu/20-SiO ₂ -used	16.0	-	-	181.5	0.50	10.6	-	8.1

^a Metal loading was measured by inductively coupled plasma atomic emission spectrometry (ICP-AES);

^b Determined by N₂O titration; ^c Calculated by the Scherrer's formula; ^d Measured by TEM.

The Brunauer–Emmett–Teller (BET) surface area, pore size, and pore volume of the calcined catalysts are also shown in Table 1. It was found that the Cu/4-SiO₂ and Cu/10-SiO₂ have high S_{BET} (472.7 and 349.4 m²/g, respectively) compared with that of Cu/20-SiO₂ (244.9 m²/g). The results show that the specific surface area of the catalyst decreases rapidly with the increase of the size of the silica sol. A larger specific surface area is beneficial to the dispersion of copper. N₂ adsorption–desorption isotherms and Barrett–Joyner–Halenda (BJH) pore size distributions of calcined catalysts are shown in Figure 1. According to the pore size distribution, the average pore diameter of Cu/*x*-SiO₂ catalysts (*x* = 4, 10, 20) were 4.6, 8.8, and 9.7 nm, and the pore volumes of catalysts were 1.05, 0.77, and 0.59 cm³·g⁻¹, respectively. It shows that all of the three catalysts have mesoporous structure, and the average pore diameter of Cu/10-SiO₂ and Cu/20-SiO₂ are obviously larger than that of Cu/4-SiO₂ catalyst. The possible reason is that appropriate mesoporous structure might be more beneficial to internal and external diffusion of reactants and products as well as the desorption. However, the average pore diameter of the catalyst is too small to be blocked during the reaction.

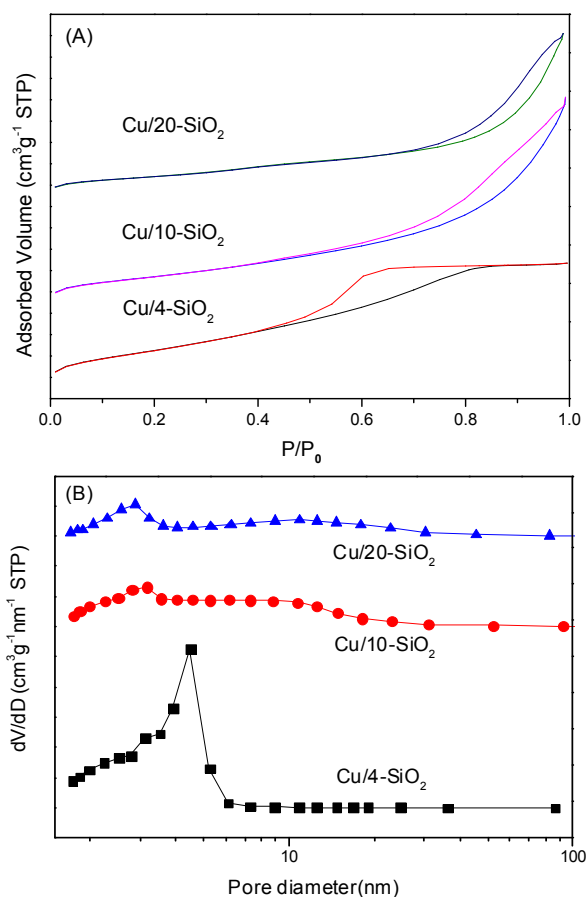


Figure 1. (A) N₂ adsorption–desorption isotherms, and (B) Brunauer–Emmett–Teller (BJH) pore size distributions of calcined catalysts.

2.2. Reducibility of the Catalysts

Temperature programmed reduction (TPR) was carried out to elucidate surface metal dispersion and metal-support interaction. Figure 2 shows the TPR profiles of the calcined (450 °C) Cu/*x*-SiO₂ catalysts. The reduction of CuO on Cu/20-SiO₂ shows two peaks, the main reduction peak at 220 °C and a broad shoulder peak at 300 °C, suggesting the presence of two kinds of particle sizes of CuO that convert into Cu; the peak at 220 °C belongs to highly dispersed CuO, and the peak at 300 °C corresponds to the reduction of large particles of copper oxide. This finding is consistent with previous findings that reduction of large particles of copper oxide occurs at 255 °C to 300 °C [17,18]. Two reduction peak are also observed in the Cu/4-SiO₂ (at 230 °C and 300 °C) and Cu/10-SiO₂ (226 °C and 300 °C) catalysts. With increasing the particle size of supports, the main reduction peaks at 220 °C to 230 °C in Cu/*x*-SiO₂ shifted to low temperatures slightly. Besides, reduction peak area at low temperature increased along with the decreasing of reduction peak area at high temperature in Cu/4-SiO₂ and Cu/10-SiO₂ catalysts compared with that of Cu/20-SiO₂ catalyst. This phenomenon may be attributed to the large particles of CuO at high reduction temperature becoming less, both Cu/4-SiO₂ and Cu/10-SiO₂ catalysts have better uniform and well-dispersed particles of copper oxide than that of Cu/20-SiO₂.

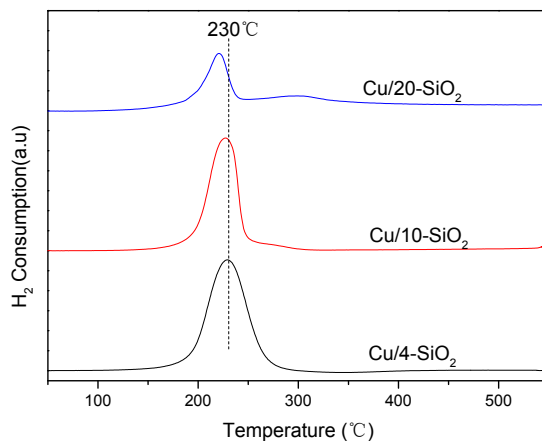


Figure 2. TPR profiles of the calcined Cu/ x -SiO₂ catalysts.

2.3. Morphology and Crystalline Phase

The x-ray diffraction (XRD) patterns of the catalysts reduced in 5% H₂/Ar mixture are shown in Figure 3. Broad peaks at 22° were observed in every catalyst which could be the amorphous silica. The diffraction peak at 2θ of 36.6° could be ascribed to Cu₂O phase (JCPDS 01-1142, JCPDS means Joint Committee on Powder Diffraction Standards), and the peak at 2θ of 43.5° along with a weak peak at 50.4° belong to Cu (JCPDS 03-1015) crystalline phases. The Cu₂O peaks gradually increased with increasing nanoparticle size of support in Cu/ x -SiO₂ catalyst. Using Scherrer equation, the calculated mean cuprous oxide crystallite sizes in Cu/ x -SiO₂ (where $x = 4, 10, 20$) catalysts were 3.3, 3.8, and 4.5 nm, respectively. Increased nanoparticle size of silica sol in the catalysts leads to increased XRD Cu₂O peaks, which may be attributed to the larger specific surface area and high dispersion of copper of Cu/4-SiO₂ and Cu/10-SiO₂ catalysts than that of Cu/20-SiO₂.

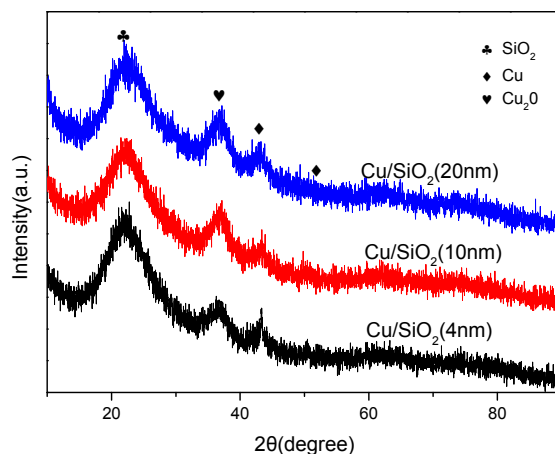


Figure 3. The x-ray diffraction (XRD) patterns of the reduced catalysts.

The transmission electron microscope (TEM) images of the reduced Cu/ x -SiO₂ in Figure 4A–C directly illustrate the effects of different nano-sized supports on the distribution of active copper particles on the catalyst surface. Numerous dark Cu nanoparticles are uniformly dispersed on the silica support surface in Figure 4A,B, while the copper species exhibited a non-uniformity dispersion in Figure 4C. The mean nanoparticle sizes of Cu on the surface of supports in Cu/ x -SiO₂ ($x = 4, 10, 20$) catalysts were 4.4, 5.4, and 5.8 nm, respectively. The mean particle size of copper was less than 6 nm, indicating a high dispersion of active metal. For the Cu/10-SiO₂ and Cu/20-SiO₂, the spherical silica supports with the diameter of about 10 nm and 20 nm could be observed, respectively. While

no obvious spherical silica support can be seen in the Cu/4-SiO₂ catalyst. The mean particle size of copper gradually increased with the increasing nano-sized silica sol support. This may be because the small size of the carrier has a larger specific surface area, which leads to an increase in the distance between the copper particles in the catalyst, thus the growth of copper particles takes longer distances and requires more energy in the process of catalytic reduction and reaction. The silica sol with small particle size restrains the migration and growth of active copper during reduction, leading to small size of the copper particles. This inference seems to be consistent with the TPR and XRD results.

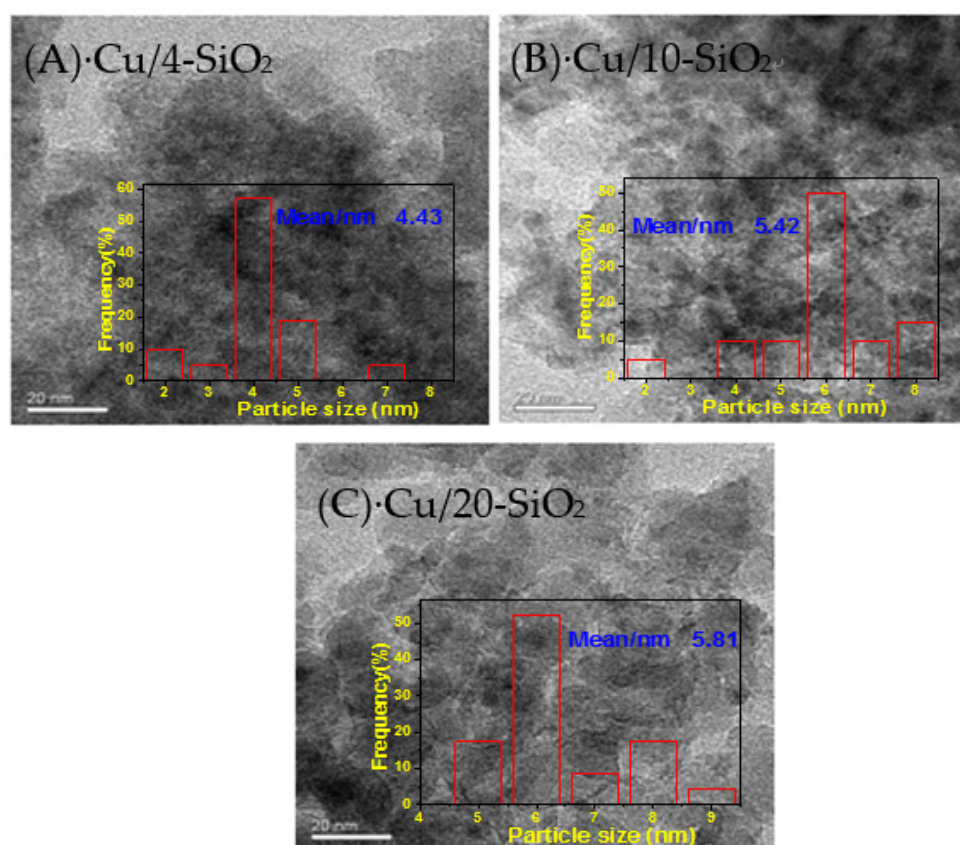


Figure 4. TEM images of the reduced Cu/*x*-SiO₂. (A) Cu/4-SiO₂; (B) Cu/10-SiO₂; (C) Cu/20-SiO₂.

2.4. Surface Composition and Chemical States

X-ray photoelectron spectroscopy (XPS) and x-ray Auger electron spectroscopy (XAES) analyses were adopted to elucidate the surface composition and surface chemical states. As shown in Table 2, surface Cu/Si molar ratio on the catalyst surface initially increases from 0.134 to 0.165, then decreases to 0.151 with the increase of the nanoparticle size of silica sol. The active component of Cu/10-SiO₂ catalyst has the best dispersion on the catalyst surface, showing that copper rearranges in the reduction process. The Cu 2p X-ray photoelectron spectra of the reduced Cu/*x*-SiO₂ catalysts are illustrated in Figure 5. The binding energies (BE) of asymmetric Cu2p_{3/2} peak can be observed in the range of 932.4 eV to 932.8 eV. The asymmetric Cu2p_{3/2} peak indicates that more than one kind of copper species with different valence states exist. The asymmetric Cu2p_{3/2} peak should be assigned to a mixture of Cu⁺ 2p_{3/2} BE and Cu⁰ 2p_{3/2} BE. The chemical states of Cu⁺ 2p_{3/2} BE and Cu⁰ 2p_{3/2} BE in the published literature are located at 932–933 eV. The differentiation of Cu⁺ and Cu⁰ from XPS is very difficult because of the peak value approach. However, XAES is a very good approach to distinguish between Cu⁰ and Cu⁺.

Table 2. X-ray photoelectron spectroscopy results of reduced Cu/*x*-SiO₂ catalysts.

Catalyst	Cu/Si (mol/mol)	BE of Cu 2p _{3/2} (eV)
Cu/4-SiO ₂	0.134	932.4
Cu/10-SiO ₂	0.165	932.5
Cu/20-SiO ₂	0.151	932.8

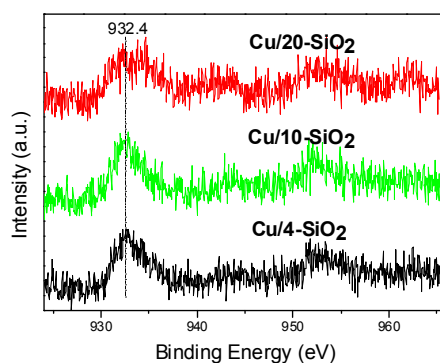
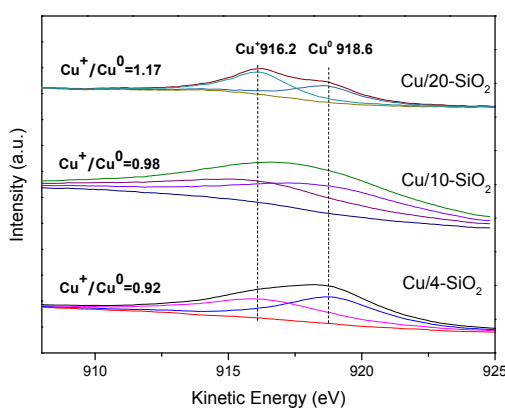
**Figure 5.** Cu2p X-ray photoelectron spectra of reduced Cu/*x*-SiO₂.

Figure 6 shows the Cu LMM of X-ray excited auger electron spectroscopy (XAES) profiles of reduced Cu/*x*-SiO₂ catalysts. The Auger kinetic energy peak is broad and asymmetric in the range of 907 eV to 925 eV. The asymmetric peak can be deconvoluted into two symmetrical peaks with centers located at the position around 916.2 and 918.6 eV, assigning to Cu⁺ and Cu⁰, respectively. The deconvolution results show that the increase in nanoparticle size of silica sol support is favorable for the formation of Cu⁺. The Cu⁺/Cu⁰ ratio of reduced Cu/*x*-SiO₂ (*x* = 4, 10 and 20 nm) catalysts were 0.92, 0.98 and 1.17, respectively. It is reported that Cu⁰ is mainly used to activate hydrogen and ester, while Cu⁺ is considered to polarize the C=O bond in the ester and contributes to the stable formation of intermediates [19]. Therefore, the appropriate Cu⁺/Cu⁰ ratio is very important for the reaction. However, there are different opinions about the proportion of Cu⁺/Cu⁰, some even opposite views [6,20]. Ma et al. consider that Cu⁰ and Cu⁺ are in a dynamic cycle during ester hydrogenation. Cu⁰ can be oxidized into Cu⁺ by ester, while H₂ can reduce Cu⁺ to Cu⁰ in the reaction [21]. Alec P. LaGrow et al. also visualized the interface transition between Cu and Cu₂O in nanoparticles with environmental scanning transmission electron microscopy (ESTEM) by switching the hydrogen and oxygen environments [22]. In view of the existence of a dynamic redox equilibrium between Cu⁰ and Cu⁺, the ratio is related to the amount of hydrogen and ester in the reaction. Therefore, it may be a reasonable choice when the Cu⁰/Cu⁺ ratio is nearly equal to one in Cu/10-SiO₂ catalyst.

**Figure 6.** Cu LMM XAES profiles of reduced Cu/*x*-SiO₂ catalysts.

2.5. Catalytic Activities

Vapor-phase DMO hydrogenation experiment was carried out to test the catalytic performance of Cu/*x*-SiO₂ catalysts. The catalytic properties under different temperatures and space velocities are listed in Table 3. EG, methyl glycolate (MG), ethanol, and other butyl glycols were the reaction products. The catalytic properties of Cu/*x*-SiO₂ catalysts are different because of the varied nanoparticle sizes of supports. Cu/10-SiO₂ and Cu/20-SiO₂ catalysts showed complete conversion, whereas the conversion of Cu/4-SiO₂ was 98.2% at the DMO WLHSV of 2.5 h⁻¹ and reaction temperature of 200 °C. The EG selectivity follows the order Cu/4-SiO₂ < Cu/20-SiO₂ < Cu/10-SiO₂. Cu/4-SiO₂ catalyst showed the lowest activity toward EG synthesis reaction. This may be attributed to the fact that Cu/4-SiO₂ catalyst has the minimum average pore diameter. Therefore, the catalyst channel is easily blocked in the reaction, which is detrimental to the diffusion of reactants and products. Cu/10-SiO₂ and Cu/20-SiO₂ catalysts have similar mesoporous structures and the average pore diameter is fairly close. Compared with Cu/20-SiO₂, the EG selectivity of Cu/10-SiO₂ is higher, which may be attributed to the smaller particle size of active copper in Cu/10-SiO₂ catalyst. The larger specific surface area of Cu/10-SiO₂ is also another factor. The selectivity of ethylene glycol in Cu/10-SiO₂ catalyst is about 94%, which should be caused by the deep hydrogenation of ethylene glycol to ethanol and others. Further research is needed to improve the selectivity, such as temperature control. It was reported that high temperature was conducive to the production of ethanol. Besides, the by-products are also useful products that will be separated in the subsequent separation process.

Table 3. Catalytic performance of Cu/*x*-SiO₂ (*x* = 4, 10, 20) for dimethyl oxalate (DMO) hydrogenation.

Samples	Temp (°C)	WLHSV _(DMO) (h ⁻¹)	Conversion (%)	Selectivity (%)				TOF ^b (h ⁻¹)
				Ethanol	MG	EG	Others ^a	
Cu/4-SiO ₂	200	2.5	98.2	1.8	27.0	70.2	1.0	-
	195	6.0	9.8	0	94.5	5.5	0	7.0
Cu/10-SiO ₂	200	2.5	100	1.3	0	94.7	4.0	-
	195	6.0	38.1	0	80.4	19.6	0	30.6
Cu/20-SiO ₂	200	2.5	100	1.9	4.4	90.7	3.0	-
	195	6.0	23.0	0	81.6	18.4	0	22.9

Reaction conditions: p(H₂) = 2.5 MPa, H₂/DMO molar ratio = 120; ^a 1,2-BDO, 1,2-PDO; ^b Turnover frequency (TOF) calculated by Cu dispersion. MG = methyl glycolate; EG = ethylene glycol.

Turnover frequency (TOF) was calculated with Cu dispersion (Table 2) [3,23], and a relatively low conversion was observed when reaction temperature was 195 °C and DMO WLHSV was 6 h⁻¹. The dispersion of copper decreased with increasing particle size of support, whereas the TOF value increased first and then decreased, and reached the maximum value of 30.6 h⁻¹ when the size of silica sol was 10 nm, suggesting that Cu/10-SiO₂ catalyst could be a better catalyst for DMO hydrogenation than Cu/20-SiO₂ and Cu/4-SiO₂.

2.6. Long-Term Experiments

Long-term experiments were carried out to study the catalytic stability and properties of Cu/*x*-SiO₂ (*x* = 4, 10, 20) catalysts. Figure 7 shows that the catalytic activity and life of Cu/4-SiO₂ catalyst is the worst when DMO WLHSV is 2.5 h⁻¹, and the catalyst begins to deactivate only for a short time. The Cu/20-SiO₂ catalyst maintained a high activity for 160 h but decreased thereafter. The Cu/10-SiO₂ catalyst showed excellent catalytic properties and stability. The conversion and EG selectivity of the Cu/10-SiO₂ catalyst slightly declined until 350 h of reaction when WLHSV was 2.5 h⁻¹. To maintain the high activity of this catalyst and to further investigate its stability, the WLHSV was adjusted to 2.25 h⁻¹ for 180 h of reaction and next to 2 h⁻¹ for 130 h of reaction when the catalytic performance of Cu/10-SiO₂ catalyst showed a slight decline. This catalyst can maintain 99.9% conversion with above 94% EG selectivity after 660 h of reaction and is still not completely inactivated and can continue to be used at lower WLHSV. The Cu/10-SiO₂ catalyst has a lifetime of over 3080 h

of reaction if it is calculated by industrial WLHSV of 0.5 h^{-1} . This characteristic can be attributed to Cu/10-SiO₂ not only having a large active copper surface area, but also to the small particle size of the Cu/10-SiO₂ support, which restrains the migration and growth of copper species in catalysts during the reaction. Cu/10-SiO₂ could be one of the best catalysts given its long life and being a good alternative for the hydrogenation of DMO to EG compared with these catalysts in the literature (Table 4). As based on calculation, the catalyst lifetime in the literature (Table 4) was generally less than 1000 hours when WLHSV_{DMO} was 0.5 h^{-1} . Moreover, the preparation method of the Cu/10-SiO₂ catalyst was also simple and did not add any additives.

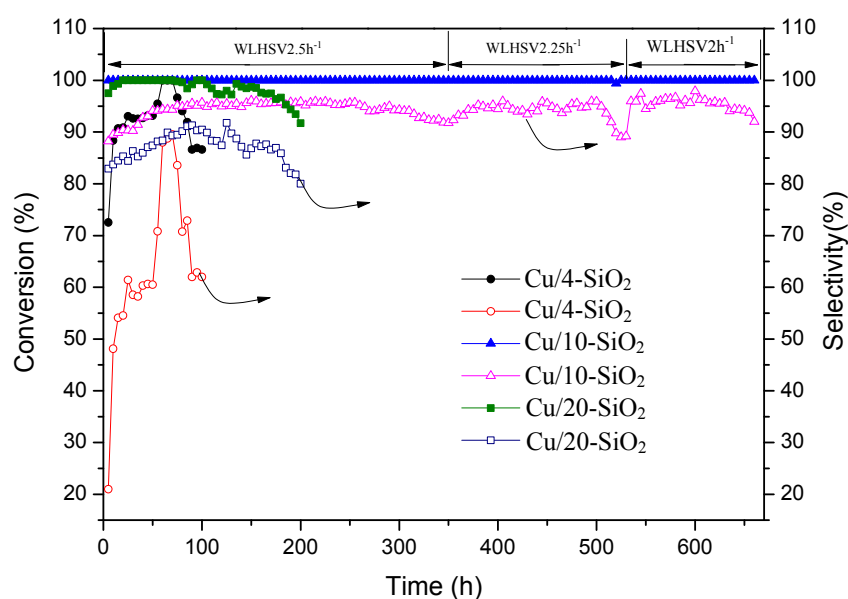


Figure 7. Long-term experiments of Cu/*x*-SiO₂ (*x* = 4, 10, 20) catalysts.

Table 4. Comparison of long-term experiments for EG synthesis from DMO.

Catalyst	Cu Loading (wt %)	Reaction Conditions	Catalytic Activity	Life Time (h)	Ref.
Cu/SiO ₂ -3 HZ-38	27.6	$p = 3 \text{ MPa}$, $T = 190 \text{ }^\circ\text{C}$, $\text{H}_2/\text{DMO} = 80$, WLHSV _(DMO) = 1.5 h^{-1} .	Conversion 99.8%, Selectivity 94.4%	300	[11]
Cu ₃ Ni/HMS	20	2.5 MPa H ₂ , 200 °C, H ₂ /DMO ratio 100, LHSV = 1.0 h^{-1}	Conversion 100%, Selectivity 98%	150	[24]
1B-Cu-SiO ₂	30	$T = 190 \text{ }^\circ\text{C}$, $p(\text{H}_2) = 3.0 \text{ MPa}$, $\text{H}_2/\text{DMO} = 80$. WLHSV _(DMO) = 0.75 h^{-1} .	conversion > 99%, Selectivity 93%	300	[25]
Cu ₁ -Ag _{0.05} /SiO ₂	10	$T = 190 \text{ }^\circ\text{C}$, $p(\text{H}_2) = 3.0 \text{ MPa}$, $\text{H}_2/\text{DMO} = 80$, WLHSV _(DMO) = 0.6 h^{-1} .	conversion 99%, Selectivity 97%	150	[26]
CuSiZr1-850	~35	$T = 190 \text{ }^\circ\text{C}$, 3 MPa, H ₂ /DMO = 150, WLHSV _(DMO) = 0.3 h^{-1} .	EG yield of > 96%	600	[6]
Cu/10-SiO ₂	16.8	$T = 200 \text{ }^\circ\text{C}$, 2.5 MPa, H ₂ /DMO = 120, WLHSV _(DMO) = 2–2.5 h ⁻¹ .	conversion > 99%, Selectivity 94%	660	This work

2.7. Characterization of the Used Catalysts

In order to demonstrate why the catalytic property and lifetime results of the catalysts differ, the TEM and S_{BET} of used catalysts (for 50 h) were also measured. Where the S_{BET} and V_p of all used catalysts decreased, the D_p values increased in Table 1. By contrast, the S_{BET} and V_p of Cu/4-SiO₂-used ($274.3 \text{ m}^2 \cdot \text{g}^{-1}$, $0.69 \text{ cm}^3 \cdot \text{g}^{-1}$) decreased significantly than those of Cu/10-SiO₂-used ($257.9 \text{ m}^2 \cdot \text{g}^{-1}$, $0.61 \text{ cm}^3 \cdot \text{g}^{-1}$) and Cu/20-SiO₂-used ($181.5 \text{ m}^2 \cdot \text{g}^{-1}$, $0.50 \text{ cm}^3 \cdot \text{g}^{-1}$) catalysts, which indicated that channels with smaller pore size are easily blocked in the reaction. The temperature programmed oxidation (TPO) experiments of used catalysts were carried out to investigate the cause of deactivation.

It can be seen from Figure S1 that the amount of carbon dioxide increased with the decreasing of particle size and average pore size of supports, which indicated that the Cu/4-SiO₂ catalyst was easier to produce carbon deposition compared with Cu/10-SiO₂ and Cu/20-SiO₂ catalysts. This may be the reason for the poor catalytic performance of Cu/4-SiO₂-used. Besides, in view of the low carbon deposition temperature (about 220 °C), the regeneration of the catalysts can be considered by calcinations.

TEM images of Cu/*x*-SiO₂-used catalysts in Figure 8 showed that partial copper particles gradually migrated and accumulated in the reaction. The mean sizes of active copper particles in the used catalysts were 5.94, 6.06, and 8.1 nm. In particular, the large copper particles on the surface of the Cu/20-SiO₂-used catalyst can be seen evidently and non-uniformly distributed. By contrast, although the copper particles on the surface of Cu/4-SiO₂-used and Cu/10-SiO₂-used were also migrated and aggregated, the copper particles size of two catalysts are still smaller than that of Cu/20-SiO₂-used catalyst. Which indicated that the small particle size of silica sol support with high specific surface area could probably limit the migration and growth of copper, in which, the increase of copper particles diameter of Cu/10-SiO₂ catalyst was the least.

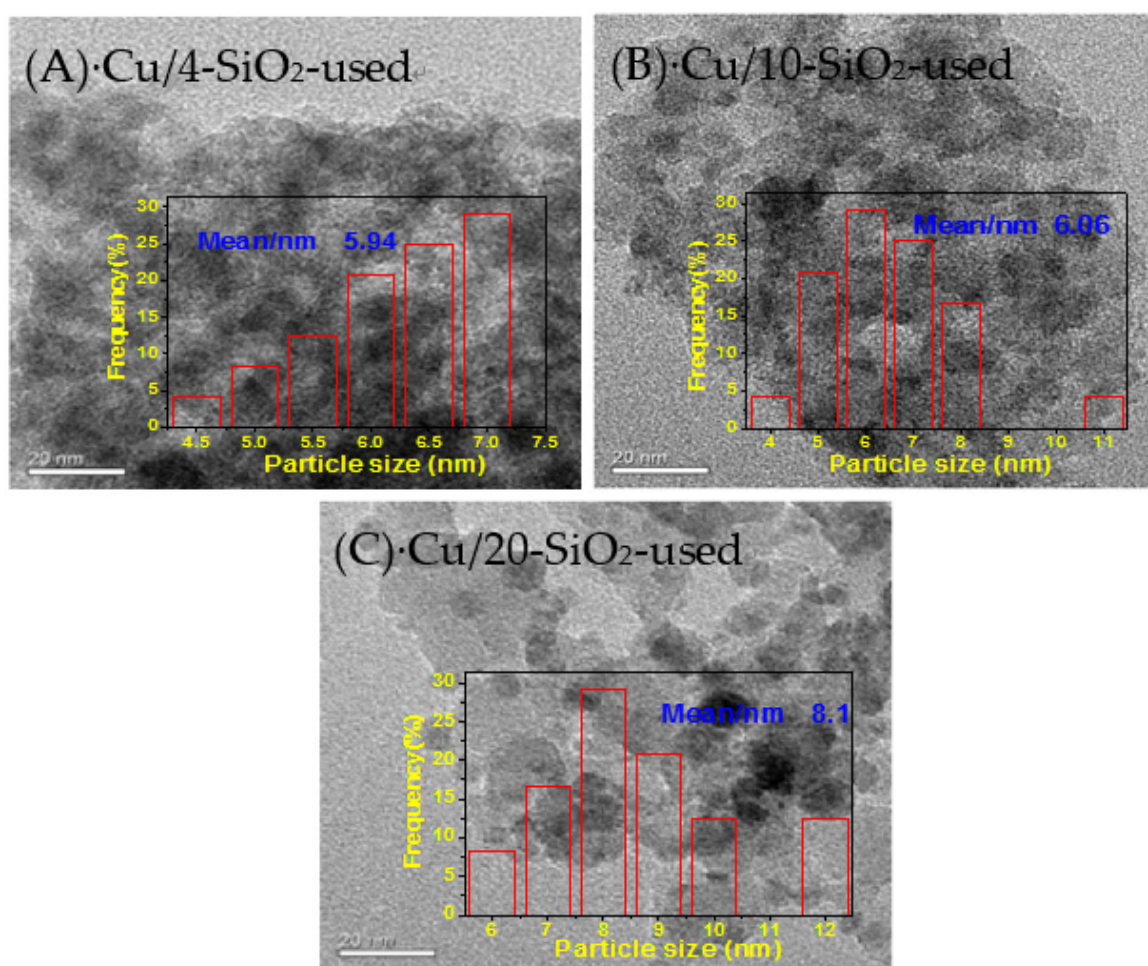


Figure 8. TEM images of used catalysts. (A) Cu/4-SiO₂-used; (B) Cu/10-SiO₂-used; (C) Cu/20-SiO₂-used.

3. Materials and Methods

3.1. Catalyst Preparation

The 20 wt % Cu/*x*-SiO₂ catalysts with different nano-sized silica sols as support materials were prepared according to an ammonia evaporation method [27], where *x* stands for the nanoparticle

size of silica sol (texture properties of silica sol are shown in Table S1 and Figure S2. About 15 g of $\text{Cu}(\text{NO}_3)_2 \cdot 3\text{H}_2\text{O}$ was dissolved in 80 mL deionized water contained in a round-bottom flask, and 45 mL of 25% to 28% ammonia aqueous solution was added into the flask and vigorously stirred for 20 min. Subsequently, different nano-sized silica sols (4, 10, and 20 nm; A.R., A Johnson Matthey Company, London, UK) containing 16 g silica were added drop-by-drop to the copper ammonia complex solution. Deionized water was added to the two other less solutions to make the three solutions of equal quality. Each solution was stirred for another 3 h at room temperature, and then the system was carried out in an oil bath at 90 °C for 4 h. The precipitate was filtered and washed thrice with a 10% ethanol aqueous solution. Blue precipitate was dried at 100 °C for 12 h and calcined at 450 °C for 5 h. The calcined catalysts were denoted as Cu/4-SiO₂, Cu/10-SiO₂, and Cu/20-SiO₂.

3.2. Characterization

N₂ adsorption–desorption measurement was conducted at −196 °C using a Micromeritics ASAP2020 instrument (Micromeritics Instrument Corporation, Norcross, GA, USA) to investigate the structural and textural properties of the samples. The copper content in the catalyst was detected by inductively coupled plasma atomic emission spectrometry (ICP-AES). X-ray diffraction (XRD; D8 Advance, Bruker Company, Karlsruhe, Germany.) patterns with Cu K α radiation at 40 kV and 40 mA were used to detect the crystalline phases of the samples. Temperature-programmed reduction (TPR) was measured by a Micromeritics ASAP2720 instrument (Micromeritics Instrument Corporation) from 25 °C to 600 °C with a heating rate of 10 °C·min^{−1}, and the flow rate of 10 vol % H₂/Ar was 40 mL·min^{−1}. TEM images were obtained using a JEM 2010 electron microscope (Japan Electron Optics Laboratory Co. Ltd, Tokyo, Japan) with an acceleration voltage of 200 kV. X-ray photoelectron spectroscopy (XPS) and Auger electron spectroscopy (XAES) were performed using an Axis Ultra spectrometer (Shimadzu Corporation, Kyoto, Japan) with a Mg K α X-ray radiation source ($h\nu = 1253.6$ eV). The metal dispersion and copper surface area of catalysts were measured by N₂O titration and hydrogen pulse reduction according to the literature [28].

3.3. Activity Measurements

The catalytic activity test was done in a fixed-bed microreactor. A 0.4 g of sample was placed in a stainless steel tubular reactor (6 mm i.d., 400 mm length). The catalyst was reduced and activated in a 5% H₂/Ar mixture gas at 300 °C for 4 h with a ramping rate of 5 °C min^{−1}. Subsequently, the system was cooled at a reaction temperature of 200 °C. Furthermore, 15 wt % DMO in methanol (via an SSI Series II pump) and H₂ were fed into the reactor with a system pressure of 2.5 MPa and a H₂/DMO molar ratio of 120. The weight liquid hourly space velocity (WLHSV) of DMO ranged from 2 h^{−1} to 6 h^{−1}. The products were cooled down and detected by a Shimadzu GC-9A gas chromatograph (Shimadzu Corporation, Kyoto, Japan) with a flame ionization detector and a 30 m Wondacap WAX wide bore capillary column (0.53 mm i. d.).

4. Conclusions

In this work, the effect of different nano-sized silica sols as supports on the structure and properties of Cu/SiO₂ for hydrogenation of dimethyl oxalate was investigated. The catalytic properties and stability of catalyst for EG synthesis follows the order Cu/4-SiO₂ < Cu/20-SiO₂ < Cu/10-SiO₂. Highly dispersed copper species, larger S_{Cu} and S_{BET} could be obtained when using 4 nm silica sol as support in Cu/4-SiO₂ catalyst, while the smaller pore size of Cu/4-SiO₂ catalyst causes the channel to be blocked very easily. Therefore, the catalytic performance of Cu/4-SiO₂ catalyst is the worst. For Cu/20-SiO₂, the lower S_{Cu} and S_{BET} , easily aggregated copper particles would result in lower catalytic activity and stability. However, Cu/10-SiO₂ catalyst not only has optimum copper surface area and S_{BET} but also the small particle size of the support in Cu/10-SiO₂, which restrains the migration and growth of copper species in catalysts during the reaction and lead to the best catalytic performance.

In addition, the Cu/10-SiO₂ catalyst still has advantages compared with these reported catalysts in Table 4.

Supplementary Materials: The following are available online at <http://www.mdpi.com/2073-4344/7/3/75/s1>, Figure S1: TPOs of the spent catalysts for 8 hours of reaction, Figure S2: (A) N₂ adsorption–desorption isotherms, and (B) BJH pore size distributions of calcined supports. Table S1: (A) N₂ adsorption–desorption isotherms, and (B) BJH pore size distributions of calcined supports.

Author Contributions: All authors contributed equally to write this article.

Conflicts of Interest: The authors declare no conflict of interest.

References

1. Chakraborty, S.; Dai, H.; Bhattacharya, P.; Fairweather, N.T.; Gibson, M.S.; Krause, J.A.; Guan, H. Iron-Based Catalysts for the Hydrogenation of Esters to Alcohols. *J. Am. Chem. Soc.* **2014**, *136*, 7869–7872. [[CrossRef](#)] [[PubMed](#)]
2. Sun, Y.; Koehler, C.; Tan, R.; Annibale, V.T.; Song, D. Ester hydrogenation catalyzed by Ru-CNN pincer complexes. *Chem. Commun.* **2011**, *47*, 8349. [[CrossRef](#)] [[PubMed](#)]
3. Ye, C.-L.; Guo, C.-L.; Zhang, J.-L. Highly active and stable CeO₂-SiO₂ supported Cu catalysts for the hydrogenation of methyl acetate to ethanol. *Fuel Process. Technol.* **2016**, *143*, 219–224. [[CrossRef](#)]
4. Yue, H.; Ma, X.; Gong, J. An alternative synthetic approach for efficient catalytic conversion of syngas to ethanol. *Accounts Chem. Res.* **2014**, *47*, 1483–1492. [[CrossRef](#)] [[PubMed](#)]
5. Zehner, L.R. Synthesis of Oxalate esters from Carbon Monoxide and Acetals or Ketals. U.S. Patent US4,005,131 A, 25 January 1977.
6. Chen, L.; Guo, P.; Qiao, M.; Yan, S.; Li, H.; Shen, W.; Xu, H.; Fan, K. Cu/SiO₂ catalysts prepared by the ammonia-evaporation method: Texture, structure, and catalytic performance in hydrogenation of dimethyl oxalate to ethylene glycol. *J. Catal.* **2008**, *257*, 172–180. [[CrossRef](#)]
7. Yue, H.; Zhao, Y.; Zhao, S.; Wang, B.; Ma, X.; Gong, J. A copper-phyllsilicate core-sheath nanoreactor for carbon-oxygen hydrogenolysis reactions. *Nat. Commun.* **2013**, *4*, 2339. [[CrossRef](#)] [[PubMed](#)]
8. Wen, C.; Li, F.; Cui, Y.; Dai, W.-L.; Fan, K. Investigation of the structural evolution and catalytic performance of the CuZnAl catalysts in the hydrogenation of dimethyl oxalate to ethylene glycol. *Catal. Today* **2013**, *10*, 75. [[CrossRef](#)]
9. Zhu, Y.; Kong, X.; Cao, D.-B.; Cui, J.; Zhu, Y.; Li, Y.-W. The Rise of Calcination Temperature Enhances the Performance of Cu Catalysts: Contributions of Support. *ACS Catal.* **2014**, *4*, 3675–3681. [[CrossRef](#)]
10. Wen, C.; Yin, A.; Cui, Y.; Yang, X.; Dai, W.-L.; Fan, K. Enhanced catalytic performance for SiO₂-TiO₂ binary oxide supported Cu-based catalyst in the hydrogenation of dimethyl oxalate. *Appl. Catal. A Gen.* **2013**, *458*, 82–89. [[CrossRef](#)]
11. Yin, A.; Wen, C.; Dai, W.-L.; Fan, K. Ag/MCM-41 as a highly efficient mesostructured catalyst for the chemoselective synthesis of methyl glycolate and ethylene glycol. *Appl. Catal. B Environ.* **2011**, *108*–*109*, 90–99. [[CrossRef](#)]
12. Zhu, Y.; Zhu, Y.; Ding, G.; Zhu, S.; Zheng, H.; Li, Y. Highly selective synthesis of ethylene glycol and ethanol via hydrogenation of dimethyl oxalate on Cu catalysts: Influence of support. *Appl. Catal. A Gen.* **2013**, *468*, 296–304. [[CrossRef](#)]
13. Yin, A.; Wen, C.; Dai, W.-L.; Fan, K. Surface modification of HMS material with silica sol leading to a remarkable enhanced catalytic performance of Cu/SiO₂. *Appl. Surf. Sci.* **2011**, *257*, 5844–5849. [[CrossRef](#)]
14. Ma, X.; Chi, H.; Yue, H.; Zhao, Y.; Xu, Y.; Lv, J.; Wang, S.; Gong, J. Hydrogenation of dimethyl oxalate to ethylene glycol over mesoporous Cu-MCM-41 catalysts. *Aiche J.* **2013**, *59*, 2530–2539. [[CrossRef](#)]
15. Lin, H.; Zheng, X.; He, Z.; Zheng, J.; Duan, X.; Yuan, Y. Cu/SiO₂ hybrid catalysts containing HZSM-5 with enhanced activity and stability for selective hydrogenation of dimethyl oxalate to ethylene glycol. *Appl. Catal. A Gen.* **2012**, *445*–*446*, 287–296. [[CrossRef](#)]
16. Guo, X.; Yin, A.; Dai, W.-L.; Fan, K. One Pot Synthesis of Ultra-High Copper Contented Cu/SBA-15 Material as Excellent Catalyst in the Hydrogenation of Dimethyl Oxalate to Ethylene Glycol. *Catal. Lett.* **2009**, *132*, 22–27. [[CrossRef](#)]
17. Chang, F.W.; Yang, H.C.; Roselin, L.S.; Kuo, W.Y. Ethanol dehydrogenation over copper catalysts on rice husk ash prepared by ion exchange. *Appl. Catal. A Gen.* **2006**, *304*, 30–39. [[CrossRef](#)]

18. Marchi, A.J.; Fierro, J.L.G.; Santamaria, J.; Monzon, A. Dehydrogenation of isopropyl alcohol on a Cu/SiO₂ catalyst: A study of the activity evolution and reactivation of the catalyst. *Appl. Catal. A* **1996**, *142*, 375–386. [[CrossRef](#)]
19. Poels, E.K.; Brands, D.S. Modification of Cu/ZnO/SiO₂ catalysts by high temperature reduction. *Appl. Catal. A* **2000**, *191*, 83. [[CrossRef](#)]
20. Yin, A.; Guo, X.; Dai, W.-L.; Fan, K. Effect of initial precipitation temperature on the structural evolution and catalytic behavior of Cu/SiO₂ catalyst in the hydrogenation of dimethyl oxalate. *Catal. Commun.* **2011**, *12*, 412–416. [[CrossRef](#)]
21. Ma, X.; Yang, Z.; Liu, X.; Tan, X.; Ge, Q. Dynamic redox cycle of Cu⁰ and Cu⁺ over Cu/SiO₂ catalyst in ester hydrogenation. *RSC Adv.* **2015**, *5*, 37581. [[CrossRef](#)]
22. LaGrow, A.P.; Ward, M.R.; Lloyd, D.C.; Gai, P.L.; Boyes, E.D. Visualizing the Cu/Cu₂O Interface Transition in Nanoparticles with Environmental Scanning Transmission Electron Microscopy. *J. Am. Chem. Soc.* **2017**, *139*, 179–185. [[CrossRef](#)] [[PubMed](#)]
23. Gong, J.; Yue, H.; Zhao, Y.; Zhao, S.; Zhao, L.; Lv, J.; Wang, S.; Ma, X. Synthesis of Ethanol via Syngas on Cu/SiO₂ Catalysts with Balanced Cu⁰–Cu⁺ Sites. *J. Am. Chem. Soc.* **2012**, *134*, 13922–13925. [[CrossRef](#)] [[PubMed](#)]
24. Yin, A.; Wen, C.; Guo, X.; Dai, W.-L.; Fan, K. Influence of Ni species on the structural evolution of Cu/SiO₂ catalyst for the chemoselective hydrogenation of dimethyl oxalate. *J. Catal.* **2011**, *280*, 77–88. [[CrossRef](#)]
25. He, Z.; Lin, H.; He, P.; Yuan, Y. Effect of boric oxide doping on the stability and activity of a Cu–SiO₂ catalyst for vapor-phase hydrogenation of dimethyl oxalate to ethylene glycol. *J. Catal.* **2011**, *277*, 54–63. [[CrossRef](#)]
26. Huang, Y.; Ariga, H.; Zheng, X.; Duan, X.; Takakusagi, S.; Asakura, K.; Yuan, Y. Silver-modulated SiO₂-supported copper catalysts for selective hydrogenation of dimethyl oxalate to ethylene glycol. *J. Catal.* **2013**, *307*, 74–83. [[CrossRef](#)]
27. Miyazaki, H.; Uda, T.; Hirai, K.; Nakamura, Y.; Ikezawa, H.; Tsuchie, T. Process for Producing Ethylene Glycol and/or Glycolic Acid Ester, Catalyst Composition Used Therefor, and Process for Production Thereof. U.S. Patent US4,585,890, 29 April 1986.
28. Zhao, S.; Yue, H.; Zhao, Y.; Wang, B.; Geng, Y.; Lv, J.; Wang, S.; Gong, J.; Ma, X. Chemoselective synthesis of ethanol via hydrogenation of dimethyl oxalate on Cu/SiO₂: Enhanced stability with boron dopant. *J. Catal.* **2013**, *297*, 142–150. [[CrossRef](#)]



© 2017 by the authors. Licensee MDPI, Basel, Switzerland. This article is an open access article distributed under the terms and conditions of the Creative Commons Attribution (CC BY) license (<http://creativecommons.org/licenses/by/4.0/>).